Effect of Dielectric Packing Materials on the Decomposition of Carbon Dioxide Using DBD Microplasma Reactor

Xiaofei Duan, Zongyuan Hu, Yanping Li, and Baowei Wang
Key Laboratory for Green Chemical Technology of the Ministry of Education, School of Chemical Engineering and Technology, Tianjin University, Tianjin 300072, China

DOI 10.1002/aic.14682
Published online November 28, 2014 in Wiley Online Library (wileyonlinelibrary.com)

Carbon dioxide (CO_2) decomposition was performed at a normal atmosphere and room temperature in dielectric barrier discharge microplasma reactors to reduce CO_2 emissions and convert CO_2 into valuable chemical materials. The outlet gases, including CO_2, CO, and O_2, were analyzed with gas chromatography. The results indicated that the conversions of CO_2 in dielectric material-packed reactors were all higher than that in nonpacked reactors. Particle size, dielectric constant, particle morphology, and acid-base properties of the dielectric materials (including quartz wool, quartz sand, γ-Al_2O_3, MgO, and CaO) all affected the CO_2 decomposition process. The conversion of CO_2 and energy efficiency achieved the highest values of 41.9 and 7.1% in a CaO-packed reactor for the higher dielectric constant and basicity of CaO. Quartz wool was also an excellent dielectric packing material because its fiber structure provided rigid sharp edges. © 2014 American Institute of Chemical Engineers *AIChE J*, 61: 898–903, 2015
Keywords: plasma, environmental engineering, CO_2 degradation, dielectric materials, packed reactor

Introduction

Over the last few decades, particular concern has been given to the effects of increases of atmospheric carbon dioxide (CO_2). CO_2 is the complete oxidation product of fossil fuels and organic compounds,[1] and CO_2 is the major contributor to the greenhouse effect because of its much greater emissions than other greenhouse gases, such as, CH_4, N_2O, SF_6, HFCs, and PFCs.[2] The growing CO_2 concentration in the atmosphere can be attributed to the burning of fossil fuels, traffic emissions, and excessive deforestation. The growing CO_2 concentration will lead to a change in the surface temperature and precipitation, which will cause lagging effects, such as, sea-level rise, and changes in hydrological and vegetation patterns.[3] There is no doubt that the treatment of CO_2 has become a worldwide problem.

Carbon capture and storage (CCS) is the most popular way to reduce CO_2 emissions, and a range of CCS technologies are under development all over the world. Gibbins and Chalmers[4] reported the main technologies for CCS in 2008. Chalmers and Gibbins[5] studied the energy consumption and CO_2 removal efficiency of CCS technologies in 2010. Kongkitisupchai and Gidaspow[6] reported CO_2 capture using solid sorbents in a fluidized bed with reduced pressure regeneration in a downer. Nevertheless, CCS is only a storing method; a high level of technological innovation and expertise are needed to control the CO_2 that enters the storage reservoir.

Correspondence concerning this article should be addressed to B. Wang at wangbw@tju.edu.cn.

CO_2 degradation, another way to handle the CO_2 emissions problem, can reduce CO_2 emissions and convert greenhouse gases to valuable chemical materials at the same time. Catalytic reaction is usually used to degrade CO_2. Usually, hydrogen (H_2) is used to hydrogenate CO_2 to methanol. The most commonly used catalysts are Cu-ZnO system catalysts.[7,8] Studt et al.[9] discovered a Ni-Ga catalyst for CO_2 reduction to methanol in 2014. However, the synthesis of catalysts is complicated and costs are high. At the same time, the reactant H_2 provides clean and efficient energy, and its production is also an urgent problem. In addition, the conventional catalytic reaction process can hardly activate CO_2 because CO_2 is thermodynamically stable.[10] Furthermore, catalytic reaction requires high temperatures, and problems of rapid deactivation due to coke and sulfur poisoning always occur.[11] A plasma-based process provides an effective way to activate CO_2 and overcomes the problems existing in the process of catalytic reaction. A plasma-based process can be an attractive way to decompose CO_2, especially when low cost and a renewable electricity source (such as, solar energy, wind resources, and hydraulic electrogeneration) is used as the plasma power supply.[12] Various plasma systems, including glow discharge plasma,[13] radio-frequency plasma,[14] gliding arc plasma,[15] capillary plasma,[16] a gas tunnel-type plasma jet,[17] and dielectric barrier discharge (DBD) plasma[18] were used to dissociate CO_2 to carbon monoxide (CO) and oxygen (O_2).

DBD plasma possesses the properties of a nonthermal plasma; DBD plasma is not in thermodynamic equilibrium and can initiate chemical reactions at unexpectedly lower temperatures than normal thermochemical reactions. DBD rarely transits to an unstable spark or arc plasma due to the presence of a dielectric barrier in the gap. DBD plasma can

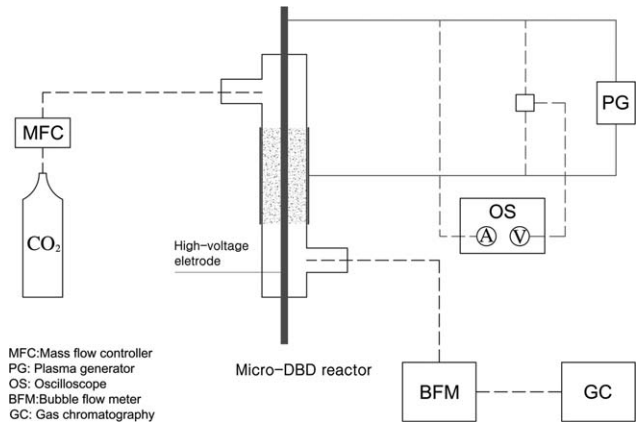

Figure 1. The schematic diagram of the experimental setup.

be operated at atmospheric pressure and is used on a large industrial scale for its low cost and ease of use.[19] Several studies of CO_2 decomposition by DBD plasma have been performed.[10,20] To improve the performance of DBD plasma in the process of CO_2 decomposition and increase the conversion of CO_2, some researchers discussed the effect of different dielectric materials that were packed in the reactor or served as a dielectric barrier. Yu et al.[21] reported the characteristics of the decomposition of CO_2 in a dielectric packed-bed plasma reactor and achieved the highest conversion value of 12.6% in a $CaTiO_3$-packed reactor. Li et al.[22] studied CO_2 decomposition using different dielectric materials in a DBD reactor, and the conversion of CO_2 reached 15.6% when $Ca_{0.7}Sr_{0.3}TiO_3$ was used as the dielectric material. DBD microplasma refers to plasma that is confined to critical dimensions below approximately 1.0 mm. With a smaller space, DBD microplasma provides a stronger electric field and higher concentration of electrons and radicals.[23] DBD microplasma combines the advantages of nonthermal plasma with those of microreactors, offering better control of processing parameters.[24]

In this study, a DBD microplasma was used to decompose pure CO_2 into CO and O_2. Quartz sand, γ-Al_2O_3, MgO, CaO, and quartz wool were packed in the discharge gap of the DBD microplasma reactor. The effect of particle size on the conversion of CO_2 was discussed. We compared and analyzed the conversions of CO_2 in reactors packed with different dielectric materials, as well as a nonpacked reactor. The effect of input power on the conversion of CO_2 and energy efficiency in a nonpacked reactor and a CaO-packed reactor was also presented.

Experimental

Dielectric materials

In this work, quartz wool (Tianjin Silicate Research Institute), quartz sand (Kemiou Chemical Reagent Co., Tianjin), γ-Al_2O_3 (Qianye Nonmetallic Material Co., China), MgO (Tianjin Guangfu Fine Chemical Research Institute), and CaO (Tianjin Guangfu Fine Chemical Research Institute) were used as dielectric packing materials, packed along the discharge area. All of these materials were commercial reagents and under no treatment. The sizes of the particles of quartz sand, γ-Al_2O_3, MgO, and CaO were in the range of 0.25–0.42 and 0.18–0.25 mm.

N_2-Physisorption analysis

N_2-Physisorption analysis of the dielectric materials was performed at −196°C on a Tristar-3000 apparatus (Micromeritics) to obtain the specific surface area, the pore volume, and the average pore diameter. Prior to the measurements, the samples were pretreated at 90°C for 3600 s under a purge of N_2, then the samples were further purged with N_2 at 300°C for 10,800 s. The specific surface areas of the samples were determined by physical adsorption of N_2 at −196°C using the Brunner–Emmet–Teller (BET) measurements equation. The pore volume was obtained from the desorption curve of the isotherm.

Experimental setup

Figure 1 shows the schematic diagram of the experimental setup, which was similar to our previous setup.[24] A DBD microplasma reactor, a flow control device, and a detection and analysis system were included in the setup. The schematic diagram of the dielectric material-packed plasma reactor is shown in Figure 2. The external aluminum foil electrode was wrapped around the outside of the quartz tube (inner diameter [I.D.] of 3.0 mm and length of 150.0 mm). A stainless steel rod with outer diameter of 1.8 mm acted as the inner electrode, generating a 0.6 mm discharge gap. The discharge length was 80.0 mm during the experiments. A plasma generator (CTP-2000, Nanjing Suman Electronic Co., China) was used to initiate the discharge. The voltage and current waveforms were measured with an oscilloscope (DPO-2012, Tektronix) using a voltage probe (P6015A, Tektronix) and a current monitor (A622, Tektronix).

Gas flow measurement and analytical system

CO_2 (99.9%) decomposition was performed under atmospheric pressure with a dielectric material-packed DBD microplasma reactor. The inlet feed gas flow rate was fixed at 3.3×10^{-7} m^3/s by a mass flow controller (MFC, D08-4C/ZM, Beijing Sevenstar Electronics Co., China). A bubble flow meter was used to calibrate the MFC and to measure the flow rate of the effluent gas.

After the start-up of the experiment, the composition of the outlet gases were analyzed using a gas chromatography (GC, Fuli 9790II, Zhejiang Fuli Analytical Instrument Co., China) every 600 s (the first sample was taken 600 s after the start-up of the experiment). The GC was equipped with a thermal conductivity detector and able to detect CO_2 and CO with a TDX-01 column (2.0 m length × 3.0 mm I.D.) and to

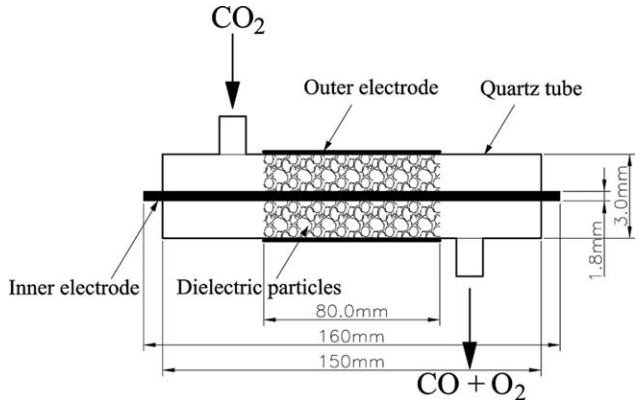

Figure 2. The schematic diagram of the dielectric material-packed plasma reactor.

Table 1. Influence of Particle Size on the Conversion of CO_2 in Different Dielectric Material-Packed Plasma Reactors

	Different Dielectric Packing Materials			
Particle Size (mm)	Quartz sand (%)	γ-Al_2O_3 (%)	MgO (%)	CaO (%)
0.25–0.42	10.3	13.6	20.5	22.6
0.18–0.25	15.2	16.3	23.7	32.8

(Feed flow rate = 3.3 × 10^{-7} m^3/s, frequency = 18.00 kHz, input power = 15.0 W, discharge gap = 0.6 mm, and external electrode length = 80.0 mm.)

detect CO and O_2 with a 5 A column (3.0 m length × 3.0 mm I.D.). He was used as its carrier gas. The evaluation of the concentration of CO_2, CO, and O_2 was accomplished using an external standard analysis method.

The conversion of CO_2, an important evaluation of system performance, was formulated by the following equation

$$X_{CO_2}(\%) = \frac{(F^{in}_{CO_2} - F^{out} \cdot C^{out}_{CO_2}) \times 100}{F^{in}_{CO_2}} \quad (1)$$

where $F^{in}_{CO_2}$ and F^{out} (m^3/s) represent the flow rate of CO_2 at the inlet of the reactor and the flow rate of effluent gas at the outlet of the reactor, respectively; $C^{out}_{CO_2}$ represents the molar fraction of CO_2 in the outlet gases, which was indicated by the GC.

The energy efficiency in this study was expressed as Eq. 2

$$\text{Efficiency}(\%) = \frac{\Delta H \times n \times 100}{P_{input} \times t} \quad (2)$$

In the reactor, the temperature was approximately 423 K. At this temperature, $\Delta H = 283.156$ kJ/mol, which is the reaction enthalpy. $n = 1$ mol, representing 1 mol CO_2 decomposition. P_{input} (W) is the total input power, and t (s) is the time of one mole of reaction.

The carbon balance (B) was calculated from the flow rate and the composition of inlet and outlet gases by Eq. 3

$$B(\%) = \frac{F^{out} \times (C^{out}_{CO} + C^{out}_{CO_2}) \times 100}{F^{in}_{CO_2}} \quad (3)$$

here C^{out}_{CO} is the molar fraction of CO in the outlet gases, which was indicated by the GC.

Results and Discussion

Effect of particle size on the conversion of CO_2

As Table 1 shows, whether the dielectric packing materials were quartz sand, γ-Al_2O_3, MgO, or CaO, the conversions of CO_2 with dielectric packing particles in the size range of 0.18–0.25 mm were much higher than with dielectric packing particles in the size range of 0.25–0.42 mm. With the same packing volume, the void fraction increased with particle size. In other words, the contact points between particles and particles/electrodes decreased with increasing particle size. Generally, the discharge takes place only in the vicinity of the contact points between the particles and particles/electrodes for the electric field strength in the contact space of the dielectric particles is much higher than the mean value in the reactor.[25] Therefore, the discharge areas in 0.18–0.25 mm dielectric particle-packed reactors were much bigger than the discharge areas in the 0.25–0.42 mm dielectric particle-packed reactors. With a higher electric field strength and larger discharge area, the conversions of CO_2 were much higher in 0.18–0.25 mm dielectric particle-packed reactors.

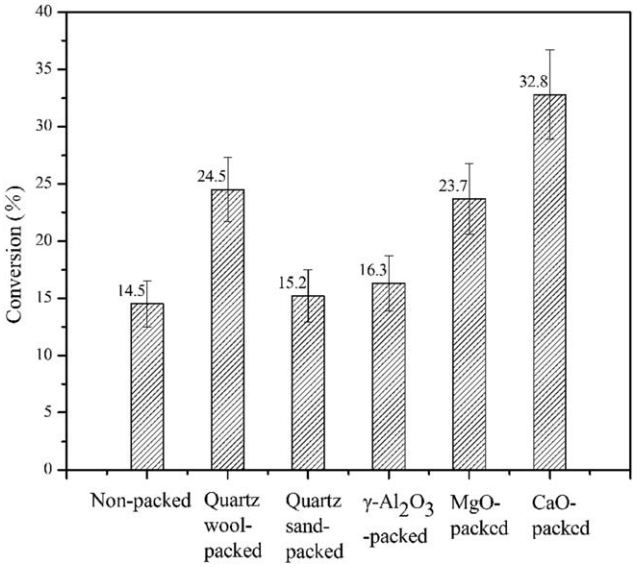

Figure 3. The conversions of CO_2 in different dielectric material-packed plasma reactors.

(Feed flow rate = 3.3 × 10^{-7} m^3/s, frequency = 18.00 kHz, input power = 15.0 W, discharge gap = 0.6 mm, and external electrode length = 80.0 mm; particle size: 0.18–0.25 mm.)

Effect of different dielectric materials on the conversion of CO_2

As Figure 3 shows, the conversions of CO_2 in dielectric material-packed reactors were all higher than the conversions of CO_2 in the nonpacked reactor. Notably, the conversion of CO_2 was highly improved in the CaO-packed reactor, and reached the highest value of 32.8%, which was approximately twice the conversion of CO_2 in the nonpacked reactor. In the quartz wool-packed reactor, the conversion of CO_2 was lower than the conversion of CO_2 in the CaO-packed reactor but higher than the conversion of CO_2 in the MgO-, γ-Al_2O_3-, and quartz sand-packed reactor. Compared with other dielectric packing materials, quartz sand and γ-Al_2O_3 had a smaller effect on the conversion of CO_2.

Table 2 shows that γ-Al_2O_3 had the largest BET surface area, and the BET surface area of CaO was the smallest. However, the conversion of CO_2 in the γ-Al_2O_3-packed reactor was much lower compared with the conversion of CO_2 in the MgO- and CaO-packed reactor. The possible reason for the differences was that the main type of adsorption of CO_2

Table 2. Dielectric Constant, BET Surface Area, Pore Volume, and Average Pore Diameter of Dielectric Packing Materials

Packing Materials	Dielectric Constant	S_{BET} (m^2/g)	Pore Diameter (nm)	Pore Volume (cm^3/g)
Quartz wool/ Quartz sand	4.60	–	–	–
γ-Al_2O_3	9.34–11.54	302.5	4.80	0.381
MgO	9.65	18.7	35.5	0.153
CaO	11.8 ± 0.3	2.10	22.4	0.022

(–) Represents that the date is not available.

Table 3. The Discharge Voltage and Current in Different Dielectric Material-Packed Plasma Reactors

	Different Dielectric Packing Materials					
	Non	Quartz Sand	Quartz Wool	γ-Al_2O_3	MgO	CaO
Discharge voltage/kV	8.40	8.42	8.91	8.67	8.73	9.13
Discharge current/A	1.84	2.31	2.47	2.11	2.49	2.52

(Feed flow rate=3.3 × 10^{-7} m^3/s, frequency=18.00 kHz, input power=15.0 W, discharge gap=0.6 mm, and external electrode length=80.0 mm; particle size=0.18–0.25 mm.)

on γ-Al_2O_3 was physisorption, while the main type of adsorption of CO_2 was chemisorption on MgO and CaO. CO_2 was more easily decomposed when it was chemically adsorbed on MgO and CaO. In addition, the result indicated that the BET surface area had little effect on the conversion of CO_2 in this work.

In the nonpacked reactor, the main discharge was uniform space discharge. When the dielectric packing materials were introduced, the primary discharge type changed to surface discharge. Surface discharge occurred along the surface of the dielectric particles. Table 3 shows the discharge voltage and current with and without dielectric packing materials. The discharge voltage and current were all higher with dielectric packing materials than without dielectric packing materials at the same input power, so the electric field strength was much higher with dielectric packing materials in the contact space. As a result, the average electron energy increased for the improvement of the electric field strength in the contact space. Therefore, the conversions of CO_2 in the dielectric material-packed reactors were all higher than in the nonpacked reactor. In addition, the electric field strength increases by increasing the dielectric constants of dielectric packing materials.[26] Therefore, dielectric packing materials with a high dielectric constant were beneficial for CO_2 conversion. Among the CaO, quartz wool, quartz sand, γ-Al_2O_3, and MgO, the dielectric constant of CaO was the highest. Hence, the conversion of CO_2 in CaO-packed reactor achieved the highest value.

The main components of quartz wool and quartz sand are all SiO_2. These materials have the same dielectric constant, which was the lowest among all the dielectric materials investigated. Quartz wool exhibited a much better effect on the conversion of CO_2 than quartz sand, even better than γ-Al_2O_3 and MgO, most likely because quartz wool was a fiber structure, which provided the quartz wool with rigid sharp edges. Chen et al.[27] reported that the sharp edges of packing particles in the plasma reactor led to higher local electric fields and highly energetic electrons. Thus, the superior performance of quartz wool relative to quartz sand, γ-Al_2O_3, and MgO in the process of CO_2 decomposition was because of its sharp edge morphology.

Meanwhile, the acid-base properties of the dielectric packing materials affected the chemisorption of CO_2 and were also a main factor in the process of CO_2 conversion. The higher basicity of the dielectric packing materials made it easier for CO_2 to adsorb on the surface of the dielectric packing materials. Consequently, the dielectric packing materials with high basicity were favorable for the adsorption of CO_2, thus facilitating CO_2 conversion. Among the dielectric packing materials investigated, CaO and MgO are basic oxides, γ-Al_2O_3 is an amphoteric oxide, and SiO_2 is an acidic oxide, and the basicity decreases in the sequence CaO > MgO > γ-Al_2O_3 > quartz wool = quartz sand. Therefore, the CaO exerted a significantly positive effect on the conversion of CO_2.

Effect of input power on CO_2 conversion in nonpacked and CaO-packed plasma reactors

Energy is the most important factor in nonthermal plasma reactions. Yu et al.[21] reported that in dielectric packed-bed plasma reactors, the dielectric properties of dielectric packing particles affect the reactions through their influence on the electron energy distribution in the plasma. In our previous work, we have also found that specific energy input (SEI) had a greater effect on the conversion of CO_2 than residence time.[24] Consequently, the effect of input power on the conversion of CO_2 and energy efficiency in the CaO-packed reactor was investigated and compared within the nonpacked reactor. CaO was selected as the dielectric packing material because it exhibited an excellent stimulative effect on the conversion of CO_2.

Figure 4 shows that the conversion of CO_2 and energy efficiency in the CaO-packed reactor was all higher than in the nonpacked reactor in the range of input power from 10.0 to 25.0 W that was investigated. For CO_2 conversion in the nonpacked reactor, the conversion of CO_2 increased from 9.3 to 14.5% with the input power increasing from 10.0 to 15.0 W, then the conversion of CO_2 remained almost unchanged with the input power further increasing to 25.0 W. The energy efficiency decreased from 3.6 to 2.2% when the input power was increased from 10.0 to 25.0 W. In the CaO-packed reactor, the conversion of CO_2 increased from 16.7 to 41.9% when the input power was increased from 10.0 to 25.0 W. The energy efficiency first increased from 5.7 to 7.1% with the input power increasing from 10.0 to 15.0 W, then decreased to 5.7% with the input power further increasing to 25.0 W.

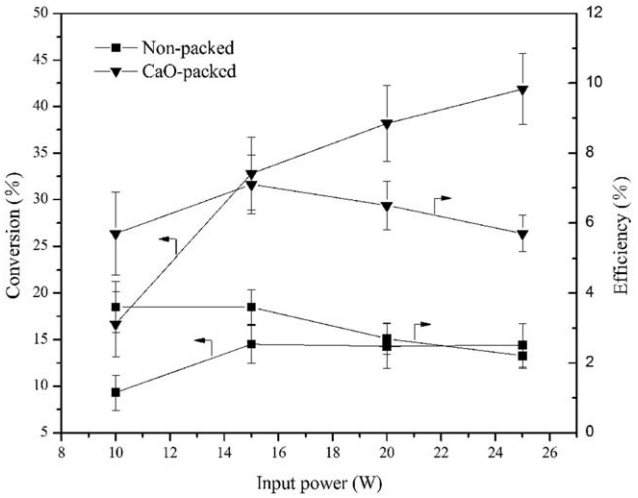

Figure 4. Influence of input power on the conversion of CO_2 and energy efficiency in nonpacked plasma reactor and CaO-packed plasma reactor.

(Feed flow rate = 3.3 × 10^{-7} m^3/s, frequency = 18.00 kHz, discharge gap = 0.6 mm, and external electrode length = 80.0 mm; particle size: 0.18–0.25 mm.)

Table 4. The Flow Rate of the Outlet Gas, Molar Fraction of CO, O_2 in the Outlet Gases, and the Carbon Balance at Different Input Power

	Non				CaO			
Input power(W)	$F^{out}(m^3/s)$	$C_{CO}^{out}(\%)$	$C_{O_2}^{out}(\%)$	B (%)	$F^{out}(m^3/s)$	$C_{CO}^{out}(\%)$	$C_{O_2}^{out}(\%)$	B (%)
10.0	3.4×10^{-7}	8.8	4.4	99.9	3.6×10^{-7}	15.3	7.6	99.8
15.0	3.5×10^{-7}	13.4	6.7	99.9	3.8×10^{-7}	28.0	14.0	99.6
20.0	3.5×10^{-7}	13.3	6.6	99.8	3.9×10^{-7}	31.9	15.9	99.5
25.0	3.5×10^{-7}	13.4	6.6	99.8	4.0×10^{-7}	34.4	17.1	99.5

F^{out} is the flow rate of the outlet gas; C_{CO}^{out} and $C_{O_2}^{out}$ represent the molar fraction of CO and O_2 in the outlet gases; and B represents the carbon balance, which was calculated by E3.
(Feed flow rate=3.3×10^{-7} m^3/s, frequency=18.00 kHz, discharge gap=0.6 mm, and external electrode length=80.0 mm; particle size=0.18–0.25 mm.)

With a higher input power, more electrons were produced with sufficient energy to activate the reactant molecules. As a result, the collision frequency between active plasma species increased, more bonds were broken and more activated radicals were produced,[28] which led to a higher CO_2 conversion. For CO_2 conversion in the nonpacked plasma reactor, the conversion of CO_2 remained almost unchanged when the input power further increased from 15.0 to 25.0 W, possibly because the reverse reaction between CO and O_2 was promoted when the input power increased as described in detail in our previous work.[24] In the CaO-packed reactor, the secondary electron emission from the dielectric materials formed surface discharges on the surface of the solid particles.[29] In the plasma, chemical reactions shifted from gas-phase reactions to heterogeneous reactions plus gas-phase reactions. Yamamoto et al.[30] reported that the heterogeneous reaction is favorable for high CO_2 conversion. In dielectric material-packed reactors, the electron energy is high but the plasma density is low, which causes a decrease in the number of microdischarges.[27] Thus, the recombination of oxide radicals was promoted in the dielectric material-packed reactor, inhibiting the reverse reaction of CO and O_2. Hence, the conversion of CO_2 increased within the range of input power in the CaO-packed reactor, while the conversion of CO_2 remained almost unchanged in the nonpacked reactor when the input power was higher than 15.0 W.

By increasing the input power, the conversion of CO_2 increased, but the energy consumed as heat increased at the same time. The two factors had reverse effects on the energy efficiency. In the nonpacked reactor, the highest value of energy efficiency was 3.6%, while the energy efficiency achieved the highest level of 7.1% in the CaO-packed reactor.

The outlet gases included CO_2, CO, and O_2, no O_3 was detected in this work. Table 4 shows the flow rate of the outlet gas, the molar fraction of CO, O_2 in the outlet gases and the carbon balance at different input power. The carbon balance was all higher than 99.5% and approached 100%. It indicated that almost all of the converted CO_2 was decomposed into CO in this work.

Mechanisms of CO_2 decomposition in the DBD plasma reactor

The process of CO_2 decomposition can be summarized in the following reaction

$$CO_2 \rightarrow CO + \frac{1}{2}O_2 \quad \Delta H = 2.8 \times 10^2 \text{ kJ/mol}$$

here CO_2, CO, and O_2 represent CO_2 molecule, CO molecule, and oxygen molecule, respectively. $\Delta H = 2.8 \times 10^2$ kJ/mol is the mole reaction enthalpy of the process.

The enthalpy of the process is fairly high; high energy is needed to decompose CO_2. Hence, it is difficult for the conventional thermal and catalytic reaction processes to activate CO_2 efficiently. The total decomposition process started with and was limited by CO_2 dissociation

$$CO_2 \rightarrow CO + O \quad \Delta H = 5.3 \times 10^2 \text{kJ/mol}$$

O represents an oxygen atom.

Then, O reacted with O into O_2 as shown in the following reactions

$$O + O \rightarrow O_2$$

$$O + CO_2 \rightarrow O_2 + CO$$

Generally, vibrational excitation of molecules, electronic excitation of molecules, and dissociative attachment of electrons are the three main channels for CO_2 dissociation. Among the three channels, vibrational excitation of molecules in the ground electronic state CO_2 ($^1\sum^+$) achieves the highest energy efficiency in nonthermal plasma.[31]

In addition to the reactions mentioned, there were also some side reactions

$$CO \rightarrow C + O \quad \Delta H = 1.0 \times 10^3 \text{ kJ/mol}$$

$$CO + O \rightarrow CO_2$$

here C is a carbon molecule.

However, CO dissociation was unlikely to be significant because of the high dissociation energy of CO. The results also verified that carbon was not produced during the reaction. The reverse reaction of CO and O was strengthened when there were more but less intense microdischarges.

When the dielectric materials were introduced into the plasma reactors, chemical reactions changed from gas-phase reactions to heterogeneous reactions and gas-phase reactions. In addition, the electric field strength and average electron energy in dielectric material-packed reactors were higher than in nonpacked reactors, facilitating the dissociation of CO_2, which was the limiting reaction of the CO_2 decomposition process and required high dissociation energy. Furthermore, some dielectric materials that were investigated, including CaO and MgO, are basic oxides, with CO_2 chemisorbed on the surface of the packing materials. As a result, breaking the C—O bond became easier and promoted the process of CO_2 decomposition. Moreover, in dielectric material-packed reactors, the environment showed fewer but more intense microdischarges, which suppressed reaction $CO + O \rightarrow CO_2$ and has a positive effect on the CO_2 conversion.

Conclusions

CO_2 decomposition through plasma provides a novel method to reduce CO_2 emissions and convert CO_2 into

valuable chemical materials at the same time. The conversion of CO_2 reached the highest value of 41.9% in a CaO-packed reactor with a feed flow rate of 3.3×10^{-7} m^3/s, input power of 25.0 W, frequency of 18.00 kHz, discharge gap of 0.6 mm, external electrode length of 80.0 mm, and particle size of 0.18–0.25 mm. CaO exhibited a superior promotional effect on the conversion of CO_2 compared with a reactor without packing materials, which achieved a conversion of CO_2 of 14.5% in the same situation. The results indicated that the particle size, dielectric constant, particle morphology, and acid-base properties of dielectric materials all affected the conversion of CO_2. The input power had a different effect on the conversion of CO_2 and energy efficiency in nonpacked and CaO-packed reactors.

Acknowledgment

Financial supports from National Natural Science Foundation of China (NSFC) under the grant of Nos. 21176175 and 20606023 are acknowledged.

Literature Cited

1. Wang JY, Xia GG, Huang A, Suib SL, Hayashi Y, Matsumoto H. CO_2 decomposition using glow discharge plasmas. *J Catal*. 1999; 185:152–159.
2. Hayashi N, Yamakawa T, Babab S. Effect of additive gases on synthesis of organic compounds from carbon dioxide using non-thermal plasma produced by atmospheric surface discharges. *Vacuum*. 2006; 80:1299–1304.
3. Ansuategi A, Escapa M. Economic growth and greenhouse gas emissions. *Ecol Econ*. 2002;40:23–37.
4. Gibbins J, Chalmers H. Carbon capture and storage. *Energy Policy*. 2008;36:4317–4322.
5. Chalmers H, Gibbins J. Carbon capture and storage: more energy or less carbon? *J Renew Sustain Energy*. 2010;2:031006.
6. Kongkitisupchai S, Gidaspow D. Carbon dioxide capture using solid sorbents in a fluidized bed with reduced pressure regeneration in a downer. *AIChE J*. 2013;59:4519–4537.
7. Arena F, Mezzatesta G, Zafarana G, Trunfio G, Frusteri F, Spadaro L. Effects of oxide carriers on surface functionality and process performance of the Cu-ZnO system in the synthesis of methanol via CO_2 hydrogenation. *J Catal*. 2013;300:141–151.
8. Arena F, Barbera K, Italiano G, Bonura G, Spadaro L, Frusteri F. Synthesis, characterization and activity pattern of Cu-ZnO/ZrO_2 catalysts in the hydrogenation of carbon dioxide to methanol. *J Catal*. 2007;249:185–194.
9. Studt F, Sharafutdinov I, Abild-Pedersen F, Elkjær CF, Hummelshøj JS, Dahl S, Chorkendorff IB, Nørskov JK. Discovery of a Ni-Ga catalyst for carbon dioxide reduction to methanol. *Nat Chem*. 2014;6:320–324.
10. Matsumoto H, Tanabe S, Okitsu K, Hayashi Y, Suib SL. Profiles of carbon dioxide decomposition in a dielectric-plasma system. *Bull Chem Soc Jpn*. 1999;72:2567–2571.
11. Li XS, Zhu B, Shi C, Xu Y, Zhu AM. Carbon dioxide reforming of methane in kilohertz spark-discharge plasma at atmospheric pressure. *AIChE J*. 2011;57:2854–2860.
12. Lebouvier A, Iwarere SA, d'Argenlieu P, Ramjugernath D, Fulcheri L. Assessment of carbon dioxide dissociation as a new route for syngas production: a comparative review and potential of plasma-based technologies. *Energy Fuels*. 2013;27:2712–2722.
13. Wang JY, Xia GG, Huang A, Suib SL, Hayashi Y, Matsumoto H. CO_2 decomposition using glow discharge plasmas. *J Catal*. 1999; 185:152–159.
14. Hsieh LT, Lee WJ, Li CT, Chen CY, Wang YF, Chang MB. Decomposition of carbon dioxide in the RF plasma environment. *J Chem Technol Biotechnol*. 1998;73:432–442.
15. Indarto A, Yang DR, Choi JW, Lee H, Song HK. Gliding arc plasma processing of CO_2 conversion. *J Hazard Mater*. 2007;146:309–315.
16. Mori S, Yamamoto A, Suzuki M. Characterization of a capillary plasma reactor for carbon dioxide decomposition. *Plasma Sources Sci Technol*. 2006;15:609–613.
17. Kobayashi A, Hamanaka H. Decomposition characteristics of carbon dioxide by gas tunnel-type plasma jet. *Vacuum*. 2006;80:1294–1298.
18. Zheng G, Jiang J, Wu Y, Zhang R, Hou H. The mutual conversion of CO_2 and CO in dielectric barrier discharge (DBD). *Plasma Chem Plasma Process*. 2003;23:59–68.
19. Kogelschatz U. Dielectric-barrier discharges: their history, discharge physics, and industrial applications. *Plasma Chem Plasma Process*. 2003;23:1–46.
20. Paulussen S, Verheyde B, Tu X, De Bie C, Martens T, Petrovic D, Bogaerts A, Sels B. Conversion of carbon dioxide to value-added chemicals in atmospheric pressure dielectric barrier discharges. *Plasma Sources Sci Technol*. 2010;19:034015 (6pp).
21. Yu QQ, Kong M, Liu T, Fei JH, Zheng XM. Characteristics of the decomposition of CO_2 in a dielectric packed-bed plasma reactor. *Plasma Chem Plasma Process*. 2012;32:153–163.
22. Li RX, Tang Q, Yin Y, Sato T. Plasma catalysis for CO_2 decomposition by using different dielectric materials. *Fuel Process Technol*. 2006;87:617–622.
23. Wang BW, Yan WJ, Ge WJ, Duan XF. Kinetic model of the methane conversion into higher hydrocarbons with a dielectric barrier discharge microplasma reactor. *Chem Eng J*. 2013;234:354–360.
24. Duan XF, Li YP, Ge WJ, Wang BW. Degradation of CO_2 through dielectric barrier discharge microplasma. *Greenhouse Gas Sci Technol*. 2014;1–10, doi: 10.1002/ghg.
25. Kang WS, Park JM, Kim Y, Hong SH. Numerical study on influences of barrier arrangements on dielectric barrier discharge characteristics. *IEEE Trans Plasma Sci*. 2003;31:504–510.
26. Chang JS, Kostov KG, Urashima K, Yamamoto T, Okayasu Y, Kato T, Iwaizumi T, Yoshimura K. Removal of NF_3 from semiconductor-process flue gases by tandem packed-bed plasma and adsorbent hybrid systems. *IEEE Trans Ind Appl*. 2000;36:1251–1259.
27. Chen HL, Lee HM, Chen SH, Chang MB. Review of packed-bed plasma reactor for ozone generation and air pollution control. *Ind Eng Chem Res*. 2008;47:2122–2130.
28. Jahanmiri A, Rahimpour MR, Shirazi M, Hooshmand N, Taghvaei H. Naphtha cracking through a pulsed DBD plasma reactor: effect of applied voltage, pulse repetition frequency and electrode material. *Chem Eng J*. 2012;191:416–425.
29. Ye QZ, Zhang T, Lu F, Li J, He ZH, Lin FH. Dielectric barrier discharge in a two-phase mixture. *J Phys D: Appl Phys*. 2008;41: 025207 (5pp).
30. Yamamoto A, Mori S, Suzuki M. Scale-up or numbering-up of a micro plasma reactor for the carbon dioxide decomposition. *Thin Solid Films*. 2007;515:4296–4300.
31. Fridman A. *Plasma Chemistry*. England: Cambridge University, 2008.

Manuscript received July 21, 2014, and revision received Nov. 4, 2014.